Plasma excitations for cylindrical nanotubes with spin splitting

2007 J. Phys.: Condens. Matter 19 106213

(http://iopscience.iop.org/0953-8984/19/10/106213)

IOP PUBLISHING JOURNAL OF PHYSICS: CONDENSED MATTER

J. Phys.: Condens. Matter **19** (2007) 106213 (10pp) doi:10.1088/0953-8984/19/10/106213

Plasma excitations for cylindrical nanotubes with spin splitting

Godfrey Gumbs, Yonatan Abranyos and Tibab McNeish

Department of Physics and Astronomy, Hunter College at the City University of New York, 695 Park Avenue New York, NY 10021, USA

E-mail: ggumbs@hunter.cuny.edu

Received 30 October 2006, in final form 5 January 2007
Published 23 February 2007
Online at stacks.iop.org/JPhysCM/19/106213

Abstract

Recent experiments have shown that a gate voltage applied perpendicular to the axis of a carbon nanotube can give rise to a spin–orbit interaction (SOI). This is of the same nature as the Rashba–Bychkov SOI at a semiconductor heterojunction and is due to the asymmetry in the confining potential of an electron on the surface of the nanotube. Using a continuum model, we obtain analytical expressions for the spin-split energy bands for electrons on the surface of nanotubes in the presence of SOI. Each energy level could then be used to accommodate electrons which could then be excited to yield intra-SO and inter-SO subband plasmons. Using numerical calculations, we present results for the plasmon dispersion relation. The anticrossing of these plasmon excitations and their group velocities are discussed.

1. Introduction

The effect of the Rashba–Bychkov [1] and Dresselhaus [2] spin–orbit interaction (SOI) on collective plasma excitations in narrow-gap heterostructures such as $In_{1-x}Ga_xAs/In_{1-x}Al_xAs$ is currently being actively investigated by several groups [3–8]. For a heterostructure, the crystal symmetry is broken at the interface where two-dimensional (2D) electrons or holes are confined in a quantum well. The resulting effect is a SO-induced splitting of the conduction/valence band into two subbands. What makes these narrow-gap semiconductors appealing as potential devices is that the SOI causes the spin to precess [9]. In [9], Datta and Das described how one may use a gate to manipulate the SOI. Recent related experiments as well as theoretical calculations on chiral nanotubes have shown that spin splitting in the absence of a magnetic field is yielded by a gate voltage applied perpendicular to the axis of the nanotube and can consequently lead to SOI [10–17]. We do not consider the intrinsic atomic SO coupling discussed by Ando [18]. The Ando SO coupling, which is independent of applied gate voltage [17], vanishes for large nanotube radii which is not the case for the Rashba coupling that we discuss in this paper.

If we are to examine how the plasma excitations are affected by the SOI on a single-wall nanotube or an array of nanotubes, we must first determine the single-particle eigenstates. Using a simple continuum model, we obtain analytical expressions for the energy bands of electrons on the surface of nanotubes with SOI. The simplified calculation we used was able to show that the SOI splits each energy level into two subbands which could then be used to accommodate the two types of spin, as is well known in two dimensions (see, for example, [19, 20]). The density of states (DOS) of the spin-split energy subbands shows that not only does the energy separation between the spin levels within a subband increase with the Rashba parameter but also as the radius of the nanotube is decreased. The DOS we obtain is in qualitative agreement with that obtained for a tight-binding model [21]. We employ our results for the single-particle eigenstates to determine the dispersion relation for the collective plasma excitations on nanotubes in the presence of SOI. We treat the system as a Landau Fermi liquid rather than as a Luttinger liquid. This is acceptable when the system is not strongly correlated, as it would be in the one-dimensional limit of small nanotube radius. We neglect disorder effects by assuming that we are dealing with high-quality nanotubes. For single-wall carbon nanotubes, the mean-free paths typically exceed 1 μm. This paper is of interest because the plasma excitation frequencies arising from intra-SO subband and inter-SO subband transitions could be in the terahertz regime. Many new devices operate in this frequency range. These include sensors and detectors for security and quantum lasers [22, 23].

In section 2 we present our model for a nanotube with the Rashba SOI present. We will treat this SOI as a coupling parameter and not explicitly include the effect of electron–electron interaction [24–26]. This model allows us to explicitly obtain analytical results for the energy bands in a tractable form. We employ these results for the energy bands to obtain the frequency- and wavevector-dependent dielectric function within the framework of the random-phase approximation (RPA) of Bohm and Pines, where each momentum transfer between electrons is treated independently. This enables us to calculate the principal effects of excitations within a SO subband and between SO subbands on the collective plasmon modes. The response function contains a form factor which is determined by the overlap of the wavefunctions for the eigenstates involved in the transition between subbands. The subbands are labelled by the angular momentum transfer quantum number $L = 0, \pm 1, \pm 2, \ldots$ arising from the cylindrical symmetry of the wavefunctions. Each of these is split by the SOI. In our numerical calculations presented in section 3 we chose $L = 0$ and found that there is an acoustic-like intra-SO (Ω_0) subband plasmon mode as well as two optic-like inter-SO (Ω_- and Ω_+) subband plasmons. The frequencies of these modes are plotted as functions of the momentum transfer q_z parallel to the axis of the nanotube. In the long-wavelength limit, $q_z \to 0$, the group velocity of the Ω_+ branch is negative whereas that for the Ω_- mode is small and positive. We conclude with some remarks in section 4.

2. The model for the spin–orbit interaction

We consider a cylindrical nanotube, with its axis on the z-axis, in the presence of a SOI. The model we employ here is for a nanotube in the presence of an applied external electric field $\mathbf{E}$ produced by a gate. This external electric field leads to an additional SOI which is different from the Ando [18] term (as discussed in the paper by De Martino and Egger [17]). The Ando SOI is independent of the gate. The form of this gate-controlled Rashba SOI in nanotubes was derived by De Martino and Egger [17]. It is a relativistic correction to the Hamiltonian which is similar to that discussed in two dimensions. Our model for the Rashba-like SOI has radial symmetry. In this case, the Hamiltonian for an electron with effective mass m^* and momentum

p on the surface of the nanotube is $H = \frac{\mathbf{p}^2}{2m^*} + \hat{H}_{\rm SO}$, where the SOI is given by

$$\hat{H}_{\rm SO} = \frac{-\hbar}{(2m^*c)^2}\mathbf{E}\cdot(\boldsymbol{\sigma}\times\mathbf{p}) = \mathrm{i}\alpha_{\rm R}\left((\sigma_1\sin\phi - \sigma_2\cos\phi)\frac{\partial}{\partial z} + \frac{\sigma_3}{R}\frac{\partial}{\partial\phi}\right). \quad (1)$$

Here, $\boldsymbol{\sigma} = (\sigma_1, \sigma_2, \sigma_3)$ are Pauli matrices and $\alpha_{\rm R}$ is the Rashba parameter for the radial confinement which is included through an electric field. We do not explicitly consider the effect of exchange interaction on $\alpha_{\rm R}$ as was discussed by Chen and Raikh [24] in a two-dimensional electron system (2DES). We simply treat $\alpha_{\rm R}$ as a parameter. Saraga and Loss [25] have also investigated the effect of screening of the Coulomb interaction for a 2DES when the SOI is included in their calculations. Hausler [26] demonstrated the role played by Coulomb interactions on the Rashba precession of spins within one-dimensional quantum channels. As the carrier density is decreased, it was found that the spin precession is enhanced when the interaction strength is increased. When a gate voltage is applied, the electric field responsible for the spin splitting will point in one direction perpendicular to the axis of the nanotube. Below, we have derived the recursive relation for the expansion coefficients for the eigenfunctions. We have also obtained the recursion relations when the electric field points in one direction only. In this case, we obtain a three-term recursive relation which can only be solved approximately when the radius of the nanotube is not too small. We have verified that the resulting energy dispersion is qualitatively similar to the radially symmetric model which we employ in this paper. Since we have only approximate results at this time which need some explanation, we present the axially symmetric model. However, both models yield qualitatively similar results for the energy dispersion for large radii. As in [1], we include the SOI through a radially *applied external* **E**. Furthermore, we use a quadratic model [27] rather than a linear model for the energy dispersion of a semi-metallic carbon nanotube without SOI [28] since we do not expect our conclusions to be affected. We note that the Rashba SOI is due to the asymmetry in the confining potential of an electron or hole gas at the interface of a heterostructure. This leads to a SOI which varies linearly with wavevector in two dimensions. The Rashba-like SOI for nanotubes is due to the asymmetry present when a gate voltage is applied. However, as we show below, the corrections to the subband energies due to SOI are not linear in the wavevector k_z.

We now write the Schrödinger equation for the total Hamiltonian and use the following to describe the spinors

$$H|u_\nu(\phi,z)\rangle = E_\nu|u_\nu(\phi,z)\rangle, \qquad |u_\nu(\phi,z)\rangle = \begin{pmatrix} u_\nu^{(+)}(\phi,z) \\ u_\nu^{(-)}(\phi,z)\end{pmatrix}. \quad (2)$$

The above equation for the eigenvalues and eigenspinors is solved with periodic boundary conditions. Since the Hamiltonian is translationally invariant along the z-axis, we seek solutions of the form $u^{(\pm)}(\phi,z) = \Phi^{(\pm)}(\phi)\mathrm{e}^{\mathrm{i}k_z z}/\sqrt{L_z}$, where L_z is a normalization length. This leads to a set of coupled ordinary differential equations, i.e.

$$-\frac{\hbar^2}{2m^*R^2}\frac{\mathrm{d}^2\Phi^{(\pm)}(\phi)}{\mathrm{d}\phi^2} + \frac{\hbar^2k_z^2}{2m^*}\Phi^{(\pm)}(\phi) - E\Phi^{(\pm)}(\phi)$$
$$= k_z\alpha_{\rm R}(\sin\phi \pm \mathrm{i}\cos\phi)\Phi^{(\mp)}(\phi) \pm \frac{\mathrm{i}\alpha_{\rm R}}{R}\frac{\mathrm{d}\Phi^{(\pm)}(\phi)}{\mathrm{d}\phi}, \quad (3)$$

where we have arranged the equations in such a way that the terms which couple them together are on the right-hand side. This arrangement separates the terms which depend on the SOI from those that do not. Indeed, if we set $\alpha_{\rm R} = 0$ it is obvious that the eigenfunctions are $\propto \mathrm{e}^{il\phi}$ with $l = 0, \pm1, \pm2, \ldots$. Furthermore, since the trigonometric functions $\sin\phi$ and $\cos\phi$ arise

from the α_R coupling, this suggests that the role played by the SOI is to mix the subbands. Consequently, we express the solutions of these coupled equations as

$$\Phi^{(\pm)}(\phi) = \sum_{l=-\infty}^{\infty} c_l^{(\pm)}(k_z)\frac{e^{il\phi}}{\sqrt{2\pi}}, \qquad \text{with } \sum_l \left|c_l^{(+)}\right|^2 + \left|c_l^{(-)}\right|^2 = 1. \tag{4}$$

Substituting the expansion for Φ into equation (3) we obtain the following relationship for the coefficients $c_l^{(\pm)}(kz)$

$$c_l^{(\pm)}(k_z) = \frac{\pm i\alpha_R k_z}{E^{(0)}(k_z, l) \mp \frac{\alpha_R l}{R} - E} c_{l\pm1}^{(\mp)}(k_z), \tag{5}$$

where

$$E^{(0)}(k_z, l) = \frac{\hbar^2 k_z^2}{2m^*} + \frac{\hbar^2 l^2}{2m^* R^2}. \tag{6}$$

We then obtain the eigenvalue equation for each subband labelled by $l = 0, \pm1, \pm2, \ldots$ to be $[(E_l^{(1)} - E)(E_{l+1}^{(2)} - E)] - \alpha_R^2 k_z^2 = 0$, yielding the energy eigenvalues

$$\begin{aligned} E^{(\pm)}(k_z, l) &= \tfrac{1}{2}\left[E_{l+1}^{(2)}(k_z) + E_l^{(1)}(k_z)\right] \pm \tfrac{1}{2}\sqrt{\left[E_{l+1}^{(2)}(k_z) - E_l^{(1)}(k_z)\right]^2 + 4\alpha_R^2 k_z^2} \\ &\equiv \frac{\hbar^2 k_z^2}{2m^*} + \frac{\hbar^2}{2m^* R^2}\left(l^2 + l + \frac{1}{2}\right) + \frac{\alpha_R}{2R} \pm \sqrt{\left(l + \frac{1}{2}\right)^2\left(\frac{\hbar^2}{2m^* R^2} + \frac{\alpha_R}{R}\right)^2 + \alpha_R^2 k_z^2}, \end{aligned} \tag{7}$$

where the second equation is obtained by making use of the defined quantities

$$\begin{aligned} &E_l^{(1)}(k_z) = E^{(0)}(k_z, l) - \frac{\alpha_R l}{R}, \qquad E_l^{(2)}(k_z) = E^{(0)}(k_z, l) + \frac{\alpha_R l}{R}, \\ &E^{(\pm)}(k_z, l) = E^{(\pm)}(k_z, -(l+1)). \end{aligned} \tag{8}$$

The eigenspinors for the corresponding energies $E^{(\pm)}(k_z, L)$ are

$$\begin{pmatrix} \Phi^{(+)}(\phi) \\ \Phi^{(-)}(\phi) \end{pmatrix}_{k_z, L}^{(\pm)} = \frac{1}{\sqrt{2\pi}} c_L^{(\pm)}(k_z) \begin{pmatrix} 1 \\ e^{i\phi}[E_L^{(1)}(k_z) - E^{(\pm)}(k_z, L)]/ik_z\alpha_R \end{pmatrix} e^{iL\phi}. \tag{9}$$

The normalization conditions give $c_L^{(+)}(k_z) = k_z\alpha_R[(E_L^{(1)} - E^{(+)}(k_z, L))^2 + k_z^2\alpha_R^2]^{-1/2}$, which we may employ to obtain $c_L^{(-)}(k_z)$ from equation (5). Thus, we have closed-form results for the eigenstates which could be used in our calculations below. Furthermore, when $\alpha_R = 0$, equation (7) reduces to $E^{(+)}(k_z, l) = E^{(0)}(k_z, l+1)$ and $E^{(-)}(k_z, l) = E^{(0)}(k_z, l)$ which are degenerate since $l = 0, \pm1, \pm2, \ldots$. Therefore, the corrections to the eigenvalues in equation (7) due to the SOI are not linear in the wavevector k_z.

The single-particle DOS is $\nu(E) = \nu_+(E) + \nu_-(E)$, where

$$\nu_\pm(E) = \frac{1}{\pi}\sqrt{\frac{\hbar^2}{2m^*}} \sum_{l=-\infty}^{\infty} \sum_{\lambda=\pm1} \frac{\Theta(K_\pm(l, E))}{\sqrt{K_\pm(l, E)}} \left\{\frac{\hbar^2}{m^*} + 2\lambda\alpha_R^2\left[B(l) + 8\alpha_R^2\frac{m^*}{\hbar^2}K_\pm(l, E)\right]^{-1/2}\right\}^{-1}, \tag{10}$$

$\Theta(x)$ is the Heaviside unit step function and

$$K_\pm(l, E) = A(l, E) + \frac{m^*\alpha_R^2}{\hbar^2} \pm \sqrt{\frac{1}{4}B(l) + \left(\frac{m^*\alpha_R^2}{\hbar^2}\right)^2 + 2A(l, E)\frac{m^*\alpha_R^2}{\hbar^2}}. \tag{11}$$

In this notation, $A(l, E) = E - \frac{\alpha_R}{2R} - \frac{\hbar^2}{4m^* R^2}(2l^2 + 2l + 1)$ $B(l) = (\frac{\alpha_R}{R} + \frac{\hbar^2}{2m^* R^2})^2(2l+1)^2$. We plot the DOS in figure 1 for a chosen nanotube radius. The separation between the spin-split

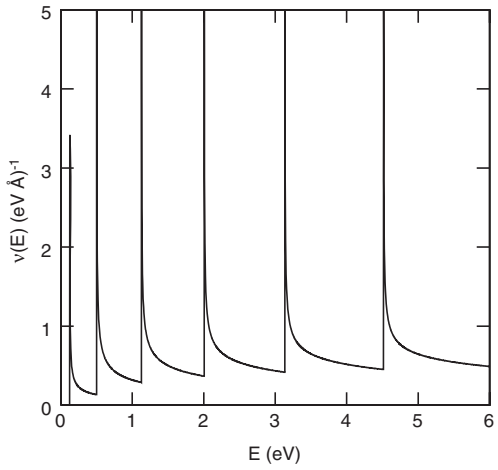

Figure 1. The total density of states $\nu(E) = \nu_+(E) + \nu_-(E)$ as a function of energy E of a single-wall nanotube of radius $R = 11.0$ Å. Here, $\alpha_R = 0.001$ meV Å, $m^* = 0.25m_e$, where m_e is the free-electron mass.

levels is decreased as the radius is increased. A calculation in the tight-binding approximation has also been presented by Kim *et al* [29] and Hertel *et al* [21]. Their result was convoluted with an energy-dependent lifetime obtained from the fast decay of photoexcited carriers.

It can be shown that in the RPA for an electron liquid on the surface of a nanotube of radius R the plasma dispersion relation can be obtained as solutions of $\epsilon_L(q,\omega) = 0$, where $\epsilon_L(q_z,\omega) = 1 + (2e^2/\epsilon_s) I_L(q_z R) K_L(q_z R) \chi_L(q_z,\omega)$. In this notation, $\chi_L(q,\omega)$ is the density–density response function resulting from electron transitions between subbands whose angular momentum quantum numbers l and l' differ by $L = l - l'$. The nanotube is embedded in a material with background dielectric constant ϵ_b and $\epsilon_s = 4\pi\epsilon_0\epsilon_b$. Also, $I_L(x)$ and $K_L(x)$ are modified Bessel functions of the first and second kind, respectively. These functions arise when the Fourier transform of the Coulomb interaction on the nanotube is taken. We have closed-form analytic expressions for the eigenvectors $|u^{(\pm)}_{k_z,l}(z,\phi)\rangle$ which can be employed to obtain

$$\chi_L(q_z,\omega) = \sum_{l,l'=-\infty}^{\infty} \sum_{\lambda,\lambda'=\pm 1} \int_{-\infty}^{\infty} \frac{dk_z}{2\pi} \frac{f_0(E^{(\lambda)}(k_z,l)) - f_0(E^{(\lambda')}(k_z - q_z, l'))}{\hbar\omega + E^{(\lambda')}(k_z - q_z, l') - E^{(\lambda)}(k_z, l)}$$
$$\times M_{\lambda\lambda'}(k_z, l; k_z - q_z, l') = \sum_{l,l'=-\infty}^{\infty} \sum_{\lambda,\lambda'=\pm 1} \int_{-\infty}^{\infty} \frac{dk_z}{2\pi} f_0(E^{(\lambda)}(k_z,l))$$
$$\times \left\{ \frac{M_{\lambda\lambda'}(k_z, l; k_z - q_z, l')}{\hbar\omega + E^{(\lambda')}(k_z - q_z, l') - E^{(\lambda)}(k_z, l)} \right.$$
$$\left. - \frac{M_{\lambda'\lambda}(k_z + q_z, l; k_z, l')}{\hbar\omega + E^{(\lambda)}(k_z, l) - E^{(\lambda')}(k_z + q_z, l')} \right\}, \tag{12}$$

where the alternative expression in equation (12) was used in doing our numerical calculations. It also shows that if the energy $E^{(\lambda)}(k_z, l)$ is below the Fermi energy, a single-particle transition to a subband with energy $E^{(\lambda')}(k_z \pm q_z, l')$ above the Fermi energy is restricted by the overlap of their wavefunctions through the form factor $M_{\lambda\lambda'}(k_z, l; k'_z, l')$ in the numerator. As a matter

of fact, the form factor is defined by

$$M_{\lambda\lambda'}(k_z,l;k'_z,l') = \left| \int_0^{2\pi} \mathrm{d}\phi\, \mathrm{e}^{\mathrm{i}L\phi} \left(\Phi^{(+)}(\phi)\ \ \Phi^{(-)}(\phi)\right)^{(\lambda)*}_{k_z,l} \begin{pmatrix} \Phi^{(+)}(\phi) \\ \Phi^{(-)}(\phi) \end{pmatrix}^{(\lambda')}_{k'_z,l'} \right|^2$$
$$= \delta_{l',l-L} \frac{\left[k_z k'_z \alpha_{\mathrm{R}}^2 + \left(E_l^{(1)}(k_z) - E^{(\lambda)}(k_z,l)\right)\left(E_{l'}^{(1)}(k'_z) - E^{(\lambda')}(k'_z,l')\right)\right]^2}{\left[k_z^2\alpha_{\mathrm{R}}^2 + \left(E_l^{(1)}(k_z) - E^{(\lambda)}(k_z,l)\right)^2\right]\left[k'^2_z\alpha_{\mathrm{R}}^2 + \left(E_{l'}^{(1)}(k'_z) - E^{(\lambda')}(k'_z,l')\right)^2\right]}. \tag{13}$$

Let us assume that $L = 0$, i.e. $l' = l$. When $q_z \to 0$, with $k'_z = k_z - q_z$, we have

$$M_{++}(k_z,l;k_z-q,l) \approx 1 - q_z \left.\frac{\mathrm{d}M_{++}(k_z,l;k_z-q,l)}{\mathrm{d}q_z}\right|_{q_z=0},$$
$$M_{+-}(k_z,l;k_z-q,l) \approx -q_z \left.\frac{\mathrm{d}M_{+-}(k_z,l;k_z-q,l)}{\mathrm{d}q_z}\right|_{q_z=0}, \tag{14}$$

with similar approximate results for $M_{--}(k_z,l;k_z-q,l)$ and $M_{-+}(k_z,l;k_z-q,l)$. These results follow from the orthonormality properties of the eigenfunctions when we set $q_z = 0$ and $L = 0$ in equation (13) and by explicitly using the eigenenergies from equation (7). The fact that M_{+-} and M_{-+} vanish as $q_z \to 0$ does not mean that there are no inter-SO subband plasma excitations in the long-wavelength limit. The reason is due to the Coulomb interaction which multiplies $\chi_{L=0}(q_z,\omega)$ in the dielectric function $\epsilon_{L=0}(q_z,\omega) = 1 + (2e^2/\epsilon_{\mathrm{s}})I_0(q_zR)K_0(q_zR)\chi_{L=0}(q_z,\omega)$ and $I_0(q_zR) \approx 1$ and $K_0(q_zR) \approx -\ln(q_zR/2)$ if $q_zR \ll 1$. When q_z increases, so that k_z and $k'_z = k_z - q_z$ differ, there is some overlap of the eigenfunctions. This means that the transitions within the same spin subband do not have the same weight as inter-SO subband transitions for the plasma excitations when $q_z = 0$. As q_z increases, the complete sets of functions $\left(\begin{smallmatrix}\Phi^{(+)}(\phi)\\ \Phi^{(-)}(\phi)\end{smallmatrix}\right)^{(\pm)}_{k_z,L}$ turn out not to be mutually orthogonal. Instead, we have $M_{++}(k_z,l;k'_z = k_z - q_z, l' = l)$ decreasing from unity such that $M_{++}(k_z,l;k'_z = k_z - q_z, l' = l) + M_{+-}(k_z,l;k'_z = k_z - q_z, l' = l) = 1$ is satisfied. Consequently, there are transitions within the same spin subband as well as between different spin subbands contributing to the response as the wavevector q_z is increased. Additional discussion of form factors and the plasma excitations they determine will be provided below when we present our numerical calculations. The limiting cases of $R \to \infty$ and $\alpha_{\mathrm{R}} \to 0$ readily follow from the above expressions [27, 30].

3. Numerical results for plasma excitations

In figure 2, we plot, at $T = 0$ K, the $L = 0$ plasma dispersion relation as a function of the reduced wavevector q_z/k_{F} for a nanotube. Here, $k_{\mathrm{F}} = \sqrt{2m^*E_{\mathrm{F}}}/\hbar$, where E_{F} is the Fermi energy. The curves were obtained by numerically calculating $\chi_{L=0}(q_z,\omega)$ in equation (12) for fixed q_z. By varying the value of ω, we were able to identify the zeros of the dielectric function $\epsilon_{L=0}(q_z,\omega)$ which correspond to the frequency of plasma excitations. We chose $\alpha_{\mathrm{R}} = 10^{-4}$ meV Å and, following [27], we set the electron effective mass as $m^* = 0.25\, m_{\mathrm{e}}$, where m_{e} is the free-electron mass, $E_{\mathrm{F}} = 0.6$ eV, the background dielectric constant $\epsilon_{\mathrm{b}} = 2.4$ and the radius of the nanotube is 11.0 Å. The plot shows three types of plasma excitation. There are low-lying intra-SO subband single-particle excitations (SPE), one acoustic-like intra-SO subband plasmon branch (Ω_0) and two inter-SO subband plasmon excitation branches (Ω_- and Ω_+). Landau damping occurs within the region where there are single-particle excitations which occurs when the plasmon branches merge with this region. The Rashba SOI gives rise to

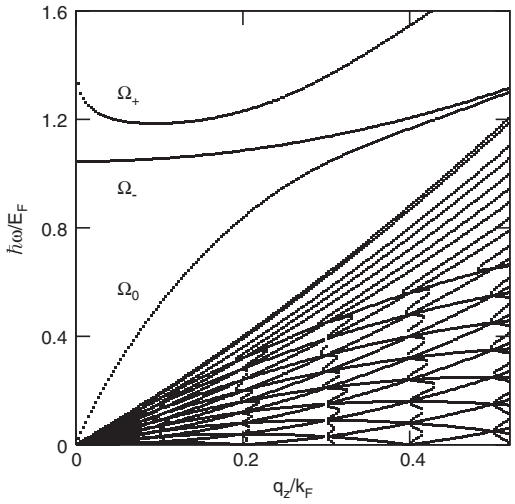

Figure 2. The plasma dispersion of the excitation energy as a function of the wavenumber $q_z/k_{\rm F}$ (in units of $k_{\rm F} = \sqrt{2m^*E_{\rm F}/\hbar^2}$) along the axis of the nanotube. We chose the Fermi energy $E_{\rm F} = 0.6$ eV, the electron effective mass $m^* = 0.25\,m_{\rm e}$ where $m_{\rm e}$ is the free-electron mass and the background dielectric constant $\epsilon_{\rm b} = 2.4$. Here, $\alpha_{\rm R} = 10^{-4}$ meV Å. The branch labelled by Ω_0 is the intra-SO plasmon. The inter-SO plasmon branches are denoted by Ω_- and Ω_+.

the two inter-SO ($\Omega_\pm$) modes. The intra-SO plasmon branch starts from the origin, increases as $\omega \propto q_z \ln(q_z R/2)$ and anticrosses with the Ω_- mode branch before it merges with the SPE spectrum at larger momentum transfer q_z where it decays into particle–hole modes. The single-particle excitation energies are shown along with those for the plasmon excitations. There is an acoustic-like plasmon branch for intra-SO subband excitations, as was obtained by Lin and Shung [27] and Gumbs and Balassis [31] for a single tubule in the absence of SO coupling. Also, figure 2 shows that there are two optic-like plasmon modes which arise from transitions between subbands. As the wavevector increases, the less energetic optic-like mode merges with the acoustic-like plasmon branch. Both of these plasmon modes are Landau damped for larger wavevectors. The optic-like mode of higher frequency (Ω_+) in figure 2 initially decreases with increasing wavevector in the long-wavelength limit. This negative (or abnormal) group velocity arises from the energy dispersion of the subbands in the presence of SOI which lifts the degeneracy of the electron states [32]. The two higher-frequency optic-like inter-SO plasmon branches anticross with each other at finite q_z. The Ω_+ plasmon wave which is of higher energy than the Ω_- branch negative group velocity in the long-wavelength limit. On the contrary, the Ω_- inter-SO subband mode has a small but positive group velocity in the long-wavelength limit, but this group velocity is increased as the transfer momentum wavevector gets larger. Consequently, for a range of values of q_z, when these two modes are excited, they transport energy in opposite directions. The Ω_+ mode transports energy in the direction opposite to the phase velocity. This phenomenon occurs over a very narrow range of frequency and only for one of the two optic-like modes. The existence of a negative group velocity depends not only on the radius of the nanotube and the electron effective mass, but also on the ratio of α/R to the Fermi energy which determines the number of occupied subbands. The magnitude of the negative group velocity is controlled by changing $\alpha/(RE_{\rm F})$. This part of the plasmon spectrum is not Landau damped by the SPE. Recently, Kushwaha and Ulloa [8] also reported on the effect which the Rashba SOI has on the group velocity of plasmon excitations in two dimensions. (For

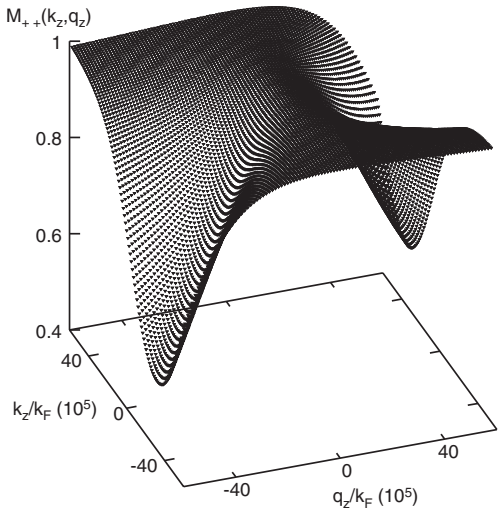

Figure 3. Three-dimensional plot of the form factor $M_{++}(k_z, q_z) \equiv M_{++}(k_z, l; k_z - q_z, l - L)$ as a function of k_z and q_z for l, $L = 0$. The radius of the nanotube is $R = 11.0$ Å and the Rashba parameter is $\alpha_R = 10^{-4}$ meV Å.

a list of references on the subject of negative group velocity, see, for example, the papers by Woodley and Mojahedi [33] and McDonald [34].) Physically, this means that there is a group delay for this collective mode over a range of wavevectors q_z.

We would like to mention that we have carried out calculations for the plasma excitation spectrum for a different set of values of α_R, the nanotube radius R as well as the electron density, i.e. the Fermi energy E_F. The details of the excitation spectrum at $T = 0$ K are determined by the subbands below the Fermi energy. In figure 2, the only subbands lying below E_F are $E^-(k_z, l = 0)$, $E^+(k_z, l = 0) = E^-(k_z, l = 1)$ and $E^+(k_z, l = 1) = E^-(k_z, l = 2)$. (We note that $E^+(k_z, l) = E^-(k_z, l + 1)$ is satisfied.) When we used a larger value of α_R, the energy subbands above E_F may also be split by the SOI. However, this is not the case for $\alpha_R = 10^{-4}$ meV Å. Thus larger α_R may lead to differences in the particle–hole regions. As a matter of fact, the lowest particle–hole excitation region in figure 2 corresponds to transitions within the $E^-(k_z, l = 0)$ subband. By plotting the energy eigenvalues as functions of wavevector, one is able to identify the branches of particle–hole excitations noting that since $L = 0$, we must have $l' = l$ for the two subbands. However, not all transitions between subbands are allowed due to the presence of the form factor $M_{\lambda\lambda'}$ in the response function. This is substantiated by the results obtained for the SPE region in figure 2 where there are gaps within the SPE region. Thus to understand the role played by the form factor, we plotted M_{++} as a function of k_z and q_z for $L = 0$ in figure 3. In essence, the physical significance of the form factor in figure 3 is to serve as a selection rule for the allowed single-particle transitions. This is governed by the wavefunction overlap in equation (13). From figure 3, we see that near $q_z = 0$, the form factor rapidly decreases to zero as k_z increases. This means that the SOI may not allow some single-particle excitations to contribute. This is consistent with the results obtained for the plasma excitation spectrum in the presence of SOI in [32], where it was found that the effect of the form factor entering the response function for a quantum wire was to disallow some of the transitions between subbands. The zeros of the denominator in the response function $\chi_L(q_z, \omega)$ give the energies of the single-particle transitions. However, because of the presence of the form factor in the denominator, similar to that appearing in equation (12), some

single-particle transitions have zero weight due to the lack of overlap between the wavefunctions for those two states involved. Tavares [35] did not include the form factor in discussing possible single-particle and collective plasmon excitations for quantum wires with SOI.

4. Concluding remarks

In summary, we have shown that although the SOI is not as large as it is for narrow-gap 2D semiconductor systems, most notably InAs, it gives rise to some interesting effects on the collective plasmon excitations on a nanotube. This includes the fact that not all single-particle transitions between subbands contribute to the collective excitations, this being determined by the degree of overlap between the eigenfunctions. The $L = 0$ plasmon excitation spectrum consists of an acoustic-like plasmon branch which is also obtained in the absence of SOI [27]. In addition, there are optic-like plasmon modes arising from inter-SO subband transitions. These are shown in figure 2, with one of the modes possessing negative group velocity in the long-wavelength limit. The acoustic-like plasmon mode splits off from the single-particle excitation region and lies above it. The optic-like plasmon modes ($\Omega_{\pm}$) split off from the inter-SO single-particle transition spectrum. Calculations may also be carried out for $L = 1$ subband transitions to yield the plasmon spectrum with SOI. Spectroscopic experiments using electron energy loss [36, 37] and Raman scattering would be useful tools for examining the results presented here.

Acknowledgments

The authors acknowledge partial support from the National Science Foundation under grant no. CREST 0206162 and PSC-CUNY Award no. 67172-00 36. GG would like to thank the Jack and Pearl Resnick Institute of Bar-Ilan University for their kind hospitality where part of this work was done. He would also like to express his thanks to the US–Israel Educational Foundation for additional financial support.

References

[1] Bychkov Yu A and Rashba E I 1984 *J. Phys. C: Solid State Phys.* **17** 6039
[2] Dresselhaus G 1955 *Phys. Rev.* **100** 580
[3] Xu W 2003 *Appl. Phys. Lett.* **82** 724
[4] Ullrich C A and Flatté M E 2002 *Phys. Rev.* B **66** 205305
Ullrich C A and Flatté M E 2003 *Phys. Rev.* B **68** 235310
[5] Gumbs G 2004 *Phys. Rev.* B **70** 235314
[6] Wang X F 2005 *Phys. Rev.* B **72** 085317
[7] Gumbs G 2005 *Phys. Rev.* B **72** 165351
[8] Kushwaha M S and Ulloa S E 2006 *Phys. Rev.* B **73** 205306
[9] Datta S and Das B 1990 *Appl. Phys. Lett.* **56** 665
[10] Mason M, Biercuk M J and Marcus C M 2004 *Science* **303** 655
[11] Tsukagoshi K, Alphenaar B W and Ago H 1999 *Nature* **401** 572
[12] Zhao B, Mönch I, Vinzelberg H, Mühl T and Schneider C M 2002 *Appl. Phys. Lett.* **80** 3144
[13] Chico L, Lopez-Sancho M P and Munoz M C 2004 *Phys. Rev. Lett.* **93** 176402
[14] Oreg Y, Byczuk K and Halperin B I 2000 *Phys. Rev. Lett.* **85** 365
[15] Entin M V and Magarill L I 2001 *Phys. Rev.* B **64** 085330
[16] Häusler W 2001 *Phys. Rev.* B **63** 121310(R)
[17] De Martino A and Egger R 2005 *J. Phys.: Condens. Matter* **17** 5523
[18] Ando T 2000 *J. Phys. Soc. Japan* **69** 1757

[19] Wang X F, Vasilopoulos P and Peeters F M 2002 *Phys. Rev.* B **65** 165217
[20] Gumbs G 2004 *Appl. Phys. Lett.* **85** 2821
[21] Hertel T, Fasel R and Moos G 2002 *Appl. Phys.* A **75** 449
[22] Kohler R, Tredicucci A, Beltram F, Beere H A, Linfield E H, Davies A G, Ritchie D A, Iotti R C and Rossi F 2002 *Nature* **417** 156
[23] Hopkins P F, Campman K L, Bellomi G, Gossard A C, Sundaram M, Yuh E L and Gwinn E G 1994 *Appl. Phys. Lett.* **64** 348
[24] Chen G-H and Raikh M E 1999 *Phys. Rev.* B **59** 5090
Chen G-H and Raikh M E 1999 *Phys. Rev.* B **60** 4826
[25] Saraga D S and Loss D 2005 *Phys. Rev.* B **72** 195319
[26] Häusler W 2001 *Phys. Rev.* B **63** 121310
[27] Lin M F and Shung K W-K 1993 *Phys. Rev.* B **47** 6617
[28] Talyanskii V I, Novikov D S, Simons B D and Levitov L S 2001 *Phys. Rev. Lett.* **87** 276802
[29] Kim P, Odom T W, Huang J-L and Lieber C M 1999 *Phys. Rev. Lett.* **82** 1225
[30] Gumbs G, Balassis A and Fekete P 2006 *Phys. Rev.* B **73** 075411
[31] Gumbs G and Balassis A 2005 *Phys. Rev.* B **71** 235410
[32] Gumbs G 2004 *Phys. Rev.* B **70** 235314
[33] Woodley J F and Mojahedi M 2004 *Phys. Rev.* E **70** 046603
[34] McDonald K T 2001 *Am. J. Phys.* **69** 607
[35] Tavares M R S 2005 *Phys. Rev.* B **72** 207302
[36] Echenique P M, Flores F and Ritchie R H 1990 *Solid State Physics: Advances in Research and Applications* vol 43, ed H Ehrenreich and D Turnbull (New York: Academic) p 230
[37] Horing N J M, Tso H C and Gumbs G 1987 *Phys. Rev.* B **36** 1588